Sparse nonlinear identification for control-oriented modeling of an Organic Rankine Cycle system

Andres Hernandez[a,*], Fredy Ruiz[b], Vincent Lemort[a]

[a] *University of Liege,Thermodynamics laboratory, Campus du Sart Tilman B49, 4000 Liege, Belgium.*
[b] *Dipartimento di Elettronica, Informazione e Bioingegneria, Politecnico di Milano, Milan, Italy*

Abstract

Accurate low-order models are essential for control and optimization of thermodynamic energy systems, yet the nonlinear and time-varying behavior of Organic Rankine Cycle (ORC) units poses a challenge for standard linear identification. This paper presents a convex sparse identification framework for nonlinear system modeling, employing a set-membership formulation to obtain compact, interpretable models with guaranteed prediction bounds. The method automatically selects the most relevant polynomial interactions from large basis functions candidates, balancing accuracy and complexity without relying on noise statistics. Experimental validation on an 11 kW_{el} ORC test bench demonstrates excellent prediction accuracy (FIT = 88.1%) with only 46 active basis functions, outperforming linear, piecewise-linear, and multiple-model Bayesian benchmarks. The identified model preserves physical interpretability through bilinear terms representing heat–flow coupling, and its compact structure is suitable for real-time model predictive control implementation.

Keywords: Nonlinear identification, Organic Rankine Cycle systems, Sparse optimization, polynomial models, NARX

1. INTRODUCTION

Climate change and the push for sustainability are driving manufacturers to seek more energy-efficient processes and reduce waste heat in vehicles and industrial systems. Waste heat recovery organic Rankine cycle (WHR-ORC) systems have emerged as a promising solution for converting low-grade heat into useful power. However, deploying these systems efficiently and cost-effectively remains a challenge, primarily due to the nonlinear and time-varying dynamics that arises under fluctuating operating conditions [1].

The performance of WHR-ORC systems depends on several factors, including the cycle configuration [2], working fluid selection [3, 4], transient response [5, 6], and particularly, the design of effective control strategies. Dynamic modeling plays a central role in enabling model-based control, which has been shown to improve operational efficiency and robustness during transients [7, 8]. A comprehensive review of dynamic modeling and control strategies for WHR-ORC systems is provided in [9].

Model Predictive Control (MPC) is one of the most promising approaches for WHR-ORC systems due to its ability to handle multivariable dynamics and operating constraints [10, 11]. The success of MPC, however, strongly depends on the availability of a reliable model that captures the system's key dynamics.

Recent advances have also demonstrated data-driven predictive control frameworks with formal stability and robustness guarantees [12], while adaptive MPC strategies continue to evolve for nonlinear and uncertain systems [13].

While physics-based models such as finite volume or moving boundary methods are well-established [14, 15], they are often too complex for real-time control applications. Hybrid approaches that combine mechanistic models with state estimators (e.g., EKF) have also been explored for MPC implementation [16].

In parallel, data-driven modeling has gained traction as a means to simplify model development while maintaining accuracy. Recent studies have leveraged machine learning and adaptive methods for ORC modeling and control. For example, [17] used neural networks to model thermodynamic properties for optimization, while [18] proposed a model-free adaptive control (MFAC) method. Additionally, [19] developed a data-driven strategy for superheating control. More recently, recurrent neural networks (RNNs) have been used in predictive control frameworks to improve modeling accuracy by incorporating structured linear transfer components [20]. Koopman operator-based approaches have also been applied to derive reduced-order models suitable for real-time MPC of WHR-ORC systems [21]. Furthermore, quasi-linear parameter-varying (QLPV) models have been developed using input–output data and Koopman-inspired techniques to support adaptive control across varying operating conditions [22]. Related learning-based MPC strategies have also been proposed, including nonlinear sparse variational Bayesian approaches for temperature control [23]. These contributions collectively highlight the increasing role of data-driven and operator-theoretic approaches in advancing ORC system performance.

An emerging direction in data-driven modeling is the use of

*Corresponding author.
Email address: jahernandez@uliege.be (Andres Hernandez)

sparse optimization techniques to derive compact, interpretable nonlinear models. Parametric identification from experimental data aims to estimate both the model structure and its parameters simultaneously [24]. Structural identification seeks to select a subset of parameters that provide a parsimonious yet informative representation of the system, facilitating control design [25]. Regularization techniques such as LASSO [26] and Elastic Net [27] enable sparse model discovery by penalizing unnecessary terms, yielding models that generalize better and are more interpretable. Recent extensions and evaluations of sparse system identification methods on nonlinear benchmarks [28] have further highlighted both the potential and the challenges of achieving robustness in data-driven models.

This concept was applied in a simulation study for ORC systems in [29], where sparse polynomial models were identified using open-loop data. However, a key limitation of that work was its sensitivity to correlated noise, which can introduce estimation bias and limit applicability in real-world systems. The present work addresses these limitations by introducing an automatic tuning strategy and a complexity-driven model selection procedure within a set-membership formulation, which enables identification from closed-loop experimental data.

In this paper, we apply the proposed sparse nonlinear identification framework to model the superheating dynamics of a WHR-ORC system using experimental data. The key idea is to approximate the nonlinear dynamics using a limited number of basis functions selected from a larger candidate set, thereby balancing prediction accuracy and model complexity. The proposed approach employs a set-membership formulation, as in [25], to enforce a predefined prediction error bound, and leverages convex optimization to identify a sparse set of model coefficients. A similar strategy has been successfully applied for controller design and filtering tasks, as shown in [30, 31]. One of the main advantages of the method of sparse identification based on set-membership is that it does not require prior assumptions about the noise distribution and can be applied to both open-loop and closed-loop datasets.

To the best of our knowledge, this is the first application of sparse nonlinear identification to WHR-ORC systems that includes experimental validation. The proposed model is evaluated on a small-scale 11 kW_{el} ORC power unit and benchmarked against established data-driven approaches, including linear modeling (LM), piecewise linear (PWL), and multiple-model Bayesian (MMB) models.

The remainder of the paper is structured as follows: Section 2 introduces the experimental ORC setup and highlights the system's key dynamic characteristics. Section 3 presents the proposed sparse identification methodology. Section 4 provides experimental validation and a comparative analysis of data-driven models. Section 5 summarizes the findings and outlines directions for future work.

2. Process description

This section outlines the architecture and key characteristics of the organic Rankine cycle (ORC) system used to evaluate the performance of the proposed modeling and identification strategies.

2.1. The Organic Rankine Cycle system

The ORC power unit analyzed in this study is a subcritical 11 kW_{el} system designed for stationary low-temperature waste heat recovery, as shown in Fig. 1. It operates on a regenerative cycle using R245fa as the working fluid. The unit includes a twin-screw expander with a nominal electrical power output of 11 kW.

Figure 1: ORC test rig.

A schematic layout of the ORC system is shown in Fig. 2. Starting from the bottom of the diagram, the liquid receiver (b) collects the saturated liquid leaving the condenser (a). From the receiver, the fluid is pumped (c) through the cold side of the regenerator (d) and then into the evaporator (e), where it is heated to a superheated vapor. The vapor then expands in the volumetric expander (f), after which it passes through the hot side of the regenerator before returning to the condenser, completing the thermodynamic cycle.

For optimal operation of the ORC unit, superheating and evaporating temperature are the most critical variables to control [32]. Superheating is defined as:

$$\Delta T_{sh} = T_{exp,su} - T_{sat,ev} \tag{1}$$

where $T_{exp,su}$ is the temperature at the expander inlet, and $T_{sat,ev}$ is the saturation temperature corresponding to the evaporator pressure $P_{sat,ev}$.

Research on ORC technology [14, 33] indicates that optimal operation of subcritical ORC systems hinges on satisfying two main criteria: **1)** Maintaining a minimum superheating level at the expander inlet ensures high efficiency and safe operation, and **2)** For each heat source condition, there exists an optimal evaporating temperature that maximizes power output. The main challenge in modeling and control arises from superheating, which displays time-varying nonlinear dynamics due

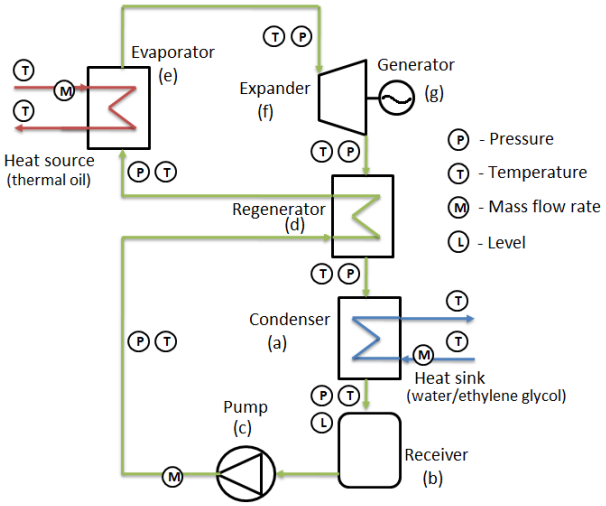

Figure 2: Process flow diagram with sensor locations.

to heat exchanger behavior and variations in the heat source [6].

2.2. Analysis of the open-loop dynamics

Previous studies have shown that optimal ORC operation occurs at low superheating values [14, 8], where the dynamics of the thermodynamic cycle are highly nonlinear and time-varying. Consequently, this work focuses on modeling the superheating degree ΔT_{sh}, with pump speed N_{pp} as the manipulated variable, and the heat source temperature T_{hf} and mass flow rate $\dot{m}_{hf}$ treated as measurable disturbances. This setup is represented schematically in Fig. 3.

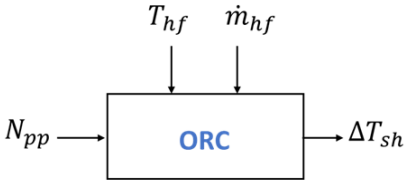

Figure 3: Block diagram of inputs and output for the ORC system.

To explore the system dynamics, step changes of 50 rpm are applied to the pump speed under different heat source conditions. Initial offsets are removed so that all responses are zero-centered, as shown in Fig. 4.

The gain, defined as $Gain = \frac{\Delta Y}{\Delta U}$, can vary by a factor of five across operating points. Similarly, the settling time—defined as the time required for the response to remain within 5% of its final value—can vary by up to a factor of seven. These substantial variations highlight the system's nonlinear behavior, primarily driven by changing heat source conditions.

The system also exhibits higher-order dynamics. This is illustrated when fitting a transfer function to some of the step responses from Fig. 4, where the model accuracy is evaluated using the Root-Mean-Square Error (RMSE) and FIT percentage [34]:

$$RMSE = \frac{\|Y - \hat{Y}\|_2}{\sqrt{L}}, \tag{2}$$

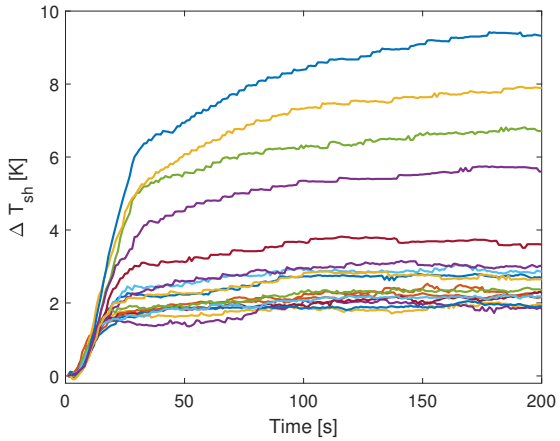

Figure 4: Superheating response to 50 rpm step changes at various operating points.

$$FIT = 100 \cdot \left(1 - \frac{\|Y - \hat{Y}\|_2}{\|Y - \text{mean}(Y)\|_2}\right), \tag{3}$$

where Y is the measured output on the validation set of length L, $\hat{Y}$ is the corresponding model prediction, and $\|\cdot\|_2$ denotes the Euclidean norm. Note that the FIT metric is a normalized prediction error measure commonly used in system identification, and differs from the coefficient of determination R^2 due to the use of Euclidean norms rather than squared errors.

At high levels of superheating, the output cannot be adequately described by a simple first-order response. As shown in Fig. 5, a third-order transfer function provides a more accurate fit to the experimental data than a standard first-order plus time delay (FOPTD) model.

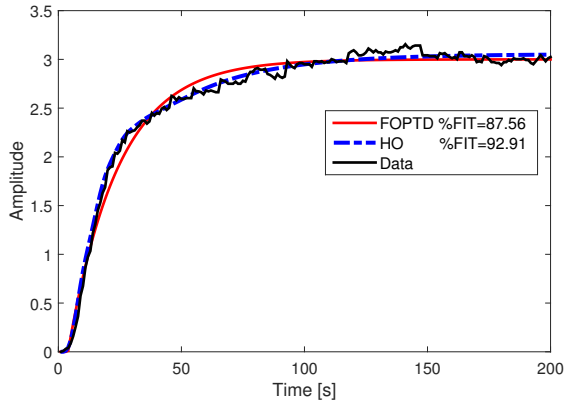

Figure 5: Comparison between FOPTD and higher-order (third-order) transfer functions at high superheating.

At low superheating levels—where nonlinearities are more pronounced—even a fourth-order model is required, as shown in Fig. 6. Increasing the model order beyond four is unnecessary, as it would introduce pole-zero cancellation without meaningful improvements in model fidelity. This analysis is also relevant for defining the regressor structure in both linear and nonlinear modeling approaches.

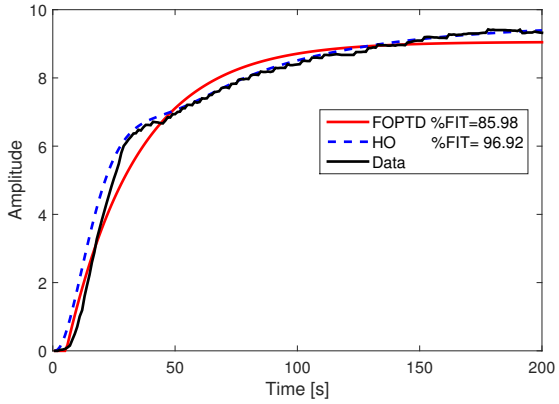

Figure 6: Comparison between FOPTD and fourth-order HO transfer functions at low superheating.

While model fits above 85% are often considered sufficient for control design—especially when robust controllers are used—our objective is different. This study aims to develop a nonlinear model that generalizes well across a wide operating range, accurately reproduces experimental data, and avoids overfitting. Such a model is suitable for both simulation purposes and advanced control strategies, including nonlinear model predictive control (NMPC).

3. The proposed Sparse Identification of Nonlinear Systems

When a reliable physics-based model is unavailable or too complex for real-time implementation, data-driven approaches provide a practical alternative for capturing system dynamics. In this section, we propose a sparse identification framework tailored to the nonlinear dynamics of the WHR-ORC system. The methodology builds upon a general ARX (AutoRegressive with eXogenous inputs) formulation and extends it into a nonlinear sparse representation using polynomial basis expansions. This hybrid strategy leverages the control-oriented structure of ARX models while embedding key thermodynamic nonlinearities through carefully selected basis functions.

3.1. ARX Model Representation

The ORC dynamics are modeled using a discrete-time multi-input single-output (MISO) ARX structure. All signals are sampled with a fixed sampling period T_s, and the discrete-time index is denoted by $k \in \mathbb{Z} \geq 0$.

The general nonlinear ARX formulation is expressed as:

$$\hat{y}(k) = \Phi(\varphi(k))^\top \theta + e(k) \tag{4}$$

where:

- $\hat{y}(k) \in \mathbb{R}$: model-predicted output,
- $\varphi(k) \in \mathbb{R}^n$: regressor vector composed of lagged inputs and outputs,
- $\Phi(\varphi(k)) \in \mathbb{R}^M$: vector of nonlinear basis functions evaluated at $\varphi(k)$, with M number of candidate functions,
- $\theta \in \mathbb{R}^M$: parameter vector to be identified,
- $e(k) \in \mathbb{R}$: bounded modeling uncertainty or disturbance.

The regressor vector $\varphi(k)$ is constructed as:

$$\varphi(k) = \begin{bmatrix} y(k-1) \\ \vdots \\ y(k-n_a) \\ u_1(k-1) \\ \vdots \\ u_1(k-n_b) \\ \vdots \\ u_{n_u}(k-1) \\ \vdots \\ u_{n_u}(k-n_b) \end{bmatrix} \tag{5}$$

where n_a is the number of output lags, n_b is the number of lags per input, and n_u is the number of input channels.

Each basis function in $\Phi(\cdot)$ represents a linear or nonlinear transformation of the regressor vector:

$$\Phi(\varphi(k)) = \begin{bmatrix} 1 \\ \varphi_1(k) \\ \varphi_2(k) \\ \varphi_1(k)^2 \\ \varphi_1(k)\varphi_2(k) \\ \vdots \end{bmatrix} \tag{6}$$

This formulation allows the representation of a wide range of nonlinear behaviors, while preserving a structure amenable to control design.

Physically, the regressor in (5) aims to capture the thermal inertia and transport delays inherent in ORC processes: lagged output terms model stored energy in heat exchangers, while lagged inputs reflect the effect of pump speed and heat-source variations propagating through the system. Whilst each of the formulation of the basis functions in (6) is flexible enough to represent cross-variable couplings (e.g., pump speed and heat-source temperature interactions) that dominate ORC nonlinearities, while remaining interpretable for control design.

For the ORC case study, the variables are defined as:

- $y(k)$: superheating degree $\Delta T_{sh}(k)$,
- $u_1(k)$: pump rotational speed $N_{pp}(k)$ (manipulated input),
- $u_2(k)$: heat-source temperature $T_{hf}(k)$ (measured disturbance),
- $u_3(k)$: heat-source mass flow rate $\dot{m}_{hf}(k)$ (measured disturbance).

Notice that the number of candidate functions M can be large, leading to overparameterization if all terms are retained. To address this, the next subsection introduces a sparse identification approach that automatically selects the most informative subset of basis functions.

3.2. Problem formulation

The goal is to identify a compact and physically interpretable nonlinear model for the ORC system, capable of accurately predicting the superheating degree ΔT_{sh} across a wide range of operating conditions.

This requirement can be formalized as a *sparse identification* problem, given:

- a dataset D of noise corrupted data consisting of input–output measurements $D = \{y(k), u_1(k), \ldots, u_{n_u}(k)\}_{k=1}^{L}$,
- a predefined set of M candidate nonlinear basis functions $\{\phi_1, \ldots, \phi_M\}$,
- a noise bound $\varepsilon > 0$,

Problem 1 (Sparse Identification)**.** *Find the sparsest parameter vector $\theta \in \mathbb{R}^M$ such that the model prediction error is compatible with the noise bound:*

$$\begin{aligned} \theta^0 = \quad & \min_{\theta \in \mathbb{R}^M} \|\theta\|_0 \\ \textit{subject to:} \quad & \|y - \Phi\theta\|_2 \leq \varepsilon \end{aligned}$$

Here, $\|\cdot\|_0$ denotes the ℓ_0 quasi-norm, defined as the number of nonzero elements in a vector:

$$\|\theta\|_0 = \mathrm{card}\,(\mathrm{supp}(\theta))$$

where

$$\mathrm{supp}(\theta) = \{i \in \{1, \ldots, M\} : \theta_i \neq 0\}$$

We now state the assumptions underlying the identification procedure:

Assumption 1. *The structure of the system is unknown but can be represented by a nonlinear mapping of the form* (4)*, inferred from input-output data.*

Assumption 2. *The true parameter vector $\theta^0 \in \mathbb{R}^M$ is sparse, i.e.,*

$$\|\theta^0\|_0 \ll M \tag{7}$$

This assumption reflects the fact that, among a large number of candidate basis functions, only a few contribute to output evolution.

Assumption 3. *The noise $e(k)$ is an unknown but bounded signal in 2-norm, i.e.,*

$$\|e\|_2 \leq \varepsilon \tag{8}$$

where the prediction error vector is the difference between the measured and the model-predicted output from (4), i.e., $e(k) = y(k) - \hat{y}(k)$.

In the ORC system, the sparsity assumption reflects the fact that only a limited number of interactions—such as $N_{pp} \cdot T_{hf}$ or $\Delta T_{sh} \cdot \dot{m}_{hf}$—are physically dominant. Most candidate polynomial terms in Φ might have negligible effect, and eliminating them improves interpretability, reduces overfitting, and preserves computational efficiency for control implementation.

Since minimization of the ℓ_0-norm is non-convex and NP-hard, the next section introduces a convex relaxation within the Set Membership Identification framework, enabling a tractable solution while maintaining the noise-bound constraint.

3.3. Sparse Set Membership Identification

Following the approach in [25], the sparse identification problem 1 is reformulated using a convex relaxation within the *Set Membership Identification* framework. The key idea is to replace the combinatorial ℓ_0-norm minimization with its convex envelope, the ℓ_1-norm, while explicitly constraining the prediction error in the ℓ_2-norm. This approach requires only an upper bound ε on the noise and modeling error, with no statistical assumptions, and ensures that all admissible solutions are consistent with both the measurements and the error bound.

Definition 1. *The* Feasible Parameter Set *(FPS) is defined as:*

$$FPS = \{\theta \in \mathbb{R}^M : \ \|y - \Phi\theta\|_2 \leq \varepsilon\}. \tag{9}$$

The FPS contains all parameter vectors that are compatible with the data, the candidate basis functions, and the prescribed noise bound.

Definition 2. *The* Feasible Sparse Parameter Set *(FSPS) is defined as:*

$$FSPS = \{\theta \in \mathbb{R}^M : \ \mathrm{supp}(\theta) = \mathrm{supp}(\theta^0), \ \|y - \Phi\theta\|_2 \leq \varepsilon\}, \tag{10}$$

where $\mathrm{supp}(\theta)$ denotes the set of indices of the nonzero coefficients. The FSPS is the subset of the FPS having exactly the same active basis functions as the true model θ^0.

Theorem 1. *Given a dataset D and a set of basis functions $\{\phi_1, \ldots, \phi_M\}$, let*

$$\begin{aligned} \varepsilon^{\min} = \quad & \min_{\theta \in \mathbb{R}^M} \quad \varepsilon \\ \textit{subject to:} \quad & \|y - \Phi\theta\|_2 \leq \varepsilon, \\ & \varepsilon \geq 0. \end{aligned} \tag{11}$$

If $\varepsilon \geq \varepsilon^{\min}$, then $FPS \neq \emptyset$.

Proof: Let θ^* be a minimizer of (11). By definition $\|y - \Phi\theta^*\|_2 \leq \varepsilon$, hence $\theta^* \in FPS$. □

In the ORC application, the FPS represents all parameter vectors that can reproduce the measured superheating degree within the combined measurement and modeling uncertainty bound ε. If the modeling assumptions hold, the true parameter vector θ^0 lies in this set.

To obtain a sparse model, Problem 1 is approximated by the following two-step procedure.

Step 1: Solve the convex optimization problem

$$\begin{aligned} \theta^1 = \quad & \min_{\theta \in \mathbb{R}^M} \quad L^{-1}\|\theta\|_1 \\ \text{subject to:} \quad & \|y - \Phi\theta\|_2 \leq \varepsilon^{(1)} \end{aligned} \tag{12}$$

where L is the number of identification samples, M is the total number of basis functions, and $\varepsilon^{(1)}$ is chosen slightly above $\varepsilon^{\min}$ (e.g., by 5%) to avoid overly restrictive feasibility conditions. The ℓ_1 term promotes sparsity by acting as the convex envelope of the ℓ_0 norm over the ℓ_∞ unit ball [27], and the ℓ_2

constraint restricts the search to the FPS [25, 35], ensuring consistency with the noise bound and a unique solution even when $M > L$.

Step 2: From θ^1, identify the set of active basis functions, and solve a reduced least-squares problem over this support:

$$\begin{aligned} \theta^* = \quad & \min_{\theta \in \mathbb{R}^M} \quad \|y - \Phi\theta\|_2 \\ \text{subject to:} \quad & \theta_i = 0 \ \ \forall i \ \ |\theta_i^1| < \gamma, \\ & \|y - \Phi\theta\|_2 \le \overline{\varepsilon} \end{aligned} \tag{13}$$

where γ is a pruning threshold that discards coefficients of negligible magnitude, and $\overline{\varepsilon} \ge \varepsilon^{(1)}$ is a relaxed error bound ensuring feasibility after pruning. This step removes the bias introduced by ℓ_1 regularization and yields an unbiased least-squares estimate on the selected support. The choice of $(\gamma, \overline{\varepsilon})$ defines the complexity–accuracy trade-off [27] and can be tuned via grid search [29] or determined automatically as described in Section 3.4.

3.4. Sparse Identification with Automatic Tuning

The feasibility of the sparse identification procedure depends critically on the choice of the error bound and pruning threshold in (12)–(13). In the manual approach of Section 3.2, these are denoted $(\gamma, \overline{\varepsilon})$ and are selected, for instance, via a grid search. Here, we introduce an *automatic tuning* strategy that replaces the manual selection of $\overline{\varepsilon}$ with a bound computed from a single scalar parameter $\zeta > 1$. This parameter scales the minimum achievable error $\varepsilon^{\min}$ from Theorem 1, thereby defining the maximum tolerated error after sparsification:

$$\varepsilon^{\max}(m_\theta) = \zeta\, \varepsilon^{\min}$$

Larger values of ζ relax the accuracy requirement and allow for sparser models, while ζ close to 1 enforces higher accuracy at the expense of complexity. This $\varepsilon^{\max}$ plays the same role in the automatic tuning scheme as $\overline{\varepsilon}$ in the two-step formulation.

To formalize the trade-off between accuracy and sparsity, we first define the notion of *model complexity*.

Definition 3. *Limited complexity model: Given a scalar $m_\theta < M$, a model f_a has* limited complexity *m_θ if $\|\theta\|_0 = m_\theta$.*

From this, we define the subset of the Feasible Parameter Set corresponding to limited complexity models compatible with the data and assumptions:

Definition 4. *Limited-complexity Feasible Parameter Set:*

$$FPS(m_\theta) = \left\{ \theta \in \mathbb{R}^M \,:\, \|y - \Phi\theta\|_2 \le \varepsilon \ \wedge \ \|\theta\|_0 = m_\theta \right\}.$$

The set $FPS(m_\theta)$ is the union of at most $\binom{M}{m_\theta}$ subsets with the same cardinality. Exhaustively testing all subsets is combinatorially intractable for large M, hence a greedy approach is adopted.

Starting from the solution $\theta^{(1)}$ obtained in Step 1 (Section 3.2), the basis functions are ranked as follows:

Definition 5. *Ordered basis index set: Let*

$$r(\theta^{(1)}) = \{i_1, \ldots, i_M : |\theta^{(1)}_{i_1}| \ge \ldots \ge |\theta^{(1)}_{i_M}|\}.$$

Here $r(\theta^{(1)})$ is the set of basis indices sorted by coefficient magnitude. For any $m_\theta \in \{1, \ldots, M\}$, the m_θ most relevant basis functions define the support

$$\lambda(m_\theta) = \{i_1, \ldots, i_{m_\theta}\}.$$

Definition 6. *Feasible Sparse Parameter Set of complexity m_θ*

$$FSPS(m_\theta) = \left\{ \theta \in \mathbb{R}^M : \|y - \Phi\theta\|_2 \le \varepsilon_s \ \wedge \ \theta_i = 0, \ \forall i \notin \lambda(m_\theta) \right\}.$$

Lemma 1. *If $\varepsilon_s \ge \varepsilon_s^{\min}(m_\theta)$, where $\varepsilon_s^{\min}(m_\theta)$ is the solution to*

$$\begin{aligned} \varepsilon_s^{\min}(m_\theta) = \quad & \min_{\theta \in \mathbb{R}^M} \quad \varepsilon \\ & \textit{subject to:} \quad \|y - \Phi\theta\|_2 \le \varepsilon, \quad \varepsilon \ge 0, \\ & \qquad\qquad \theta_i = 0, \ \forall i \notin \lambda(m_\theta), \end{aligned}$$

then $FSPS(m_\theta) \neq \emptyset$.

Corollary 1. *Let $\varepsilon(m_\theta) = \varepsilon_s^{\min}(m_\theta) - \varepsilon^{\min}$. Then $\varepsilon(m_\theta) \ge 0$, and if $\varepsilon(m_\theta) = 0$, it follows that $FSPS(m_\theta) \subset FPS$.*

Remark 1. *If $\varepsilon(m_\theta) = 0$, the reduced set of m_θ basis functions achieves the same minimum prediction error as the full set, making $\varepsilon(m_\theta)$ a direct indicator of the accuracy–sparsity trade-off.*

Once the desired support $\lambda(m_\theta)$ is fixed, the final parameter vector $\hat{\theta}$ is obtained as

$$\begin{aligned} \hat{\theta} = \quad & \min_{\theta \in \mathbb{R}^M} \quad \|y - \Phi\theta\|_2 \\ \text{subject to:} \quad & \theta_i = 0, \ \forall i \notin \lambda(m_\theta). \end{aligned} \tag{14}$$

Algorithm 1. Sparse Set Membership Nonlinear Algorithm with Automatic Tuning

1. Collect a dataset D from experiments covering the operational range of the ORC. Input signals must ensure persistence of excitation. Both open- and closed-loop data are admissible.
2. Select a set of candidate basis functions $\Phi(\varphi(k)) \in \mathbb{R}^M$.
3. Compute the minimum achievable error $\varepsilon^{\min}$ via Theorem 1.
4. Solve:

$$\begin{aligned} \theta^{(1)} = \quad & \min_{\theta \in \mathbb{R}^M} \quad L^{-1}\|\theta\|_1 \\ \text{subject to:} \quad & \|y - \Phi\theta\|_2 \le \varepsilon^{(1)} \end{aligned}$$

   where $\varepsilon^{(1)}$ is typically $1.05\,\varepsilon^{\min}$.
5. Rank basis functions using $r(\theta^{(1)})$ from Definition 5.
6. Perform the following iteration,
   For $j = 1$ to $M - 1$:
   a. Set $m_\theta = M - j$ and $\varepsilon^{\max}(m_\theta) = \zeta\, \varepsilon^{\min}$.
   b. Solve the least-squares problem restricted to $\lambda(m_\theta)$.

c. If the achieved error $\leq \varepsilon^{\max}(m_\theta)$, set $\hat{\theta} = \theta(j)$ and continue; otherwise, terminate.

Remark 2. *The parameter ζ is the* only *tuning knob controlling the sparsity–accuracy balance in the automatic procedure. Small ζ yields denser models with higher accuracy, while larger ζ allows fewer active terms with a controlled accuracy loss.*

For clarity, Fig. 7 provides a high-level overview of the proposed sparse nonlinear identification procedure. The flowchart summarizes the main steps of Algorithm 1, from data acquisition and basis function construction to sparsity tuning, model selection, and validation. It is intended to guide the reader through the overall workflow, while the detailed mathematical formulation is given in the preceding sections.

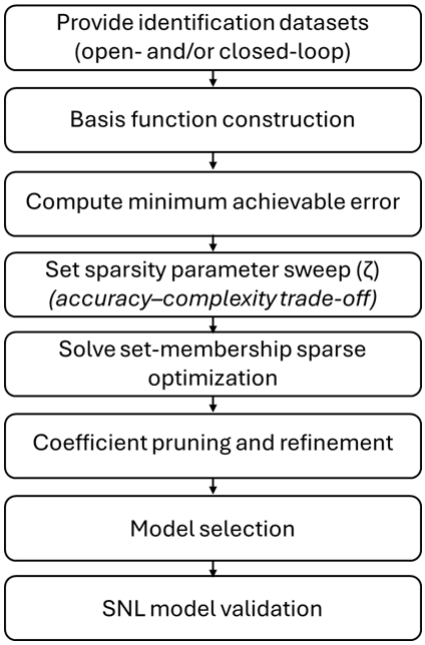

Figure 7: Flowchart of the proposed sparse nonlinear identification procedure for WHR-ORC systems.

3.5. Computational complexity and scalability

The proposed sparse identification algorithm is solved offline, and its computational cost is dominated by the convex optimization problem used for structure selection. Let M denote the number of candidate basis functions and L the number of data samples. The initial set-membership optimization in (12) involves an ℓ_1-norm minimization with an ℓ_2 constraint over M decision variables, whose computational complexity scales polynomially with M and depends on L through the evaluation of the prediction error constraint. In practice, this problem is efficiently handled by modern interior-point solvers.

Once a sparse solution is obtained, the subsequent refinement and pruning steps operate on a significantly reduced set of active basis functions $m_\theta \ll M$, making their computational cost negligible in comparison. Importantly, model evaluation scales linearly with m_θ, which enables efficient real-time execution even when large candidate libraries are considered during the offline identification phase. This separation between offline identification and online model evaluation ensures scalability of the proposed approach to higher-dimensional basis function libraries.

4. Experimental Results and Discussion

Low-order dynamic models are valuable for simulation, optimization, and control of ORC systems. However, a balance must be struck between model complexity and prediction accuracy, especially when the model is intended for control-oriented applications. In this section, we present the identification and evaluation of a sparse nonlinear (SNL) polynomial model for predicting the superheating degree, ΔT_{sh}, across a wide range of operating conditions.

4.1. Sparse Nonlinear Identification Experiment

The basis function library was constructed by incorporating known physical relationships of the WHR-ORC process. Specifically, ΔT_{sh} depends nonlinearly on the manipulated variable (pump speed N_{pp}) and on measured disturbances representing the heat source conditions: the heat source temperature T_{hf} and mass flow rate $\dot{m}_{hf}$. Quadratic and bilinear interaction terms (e.g., $N_{pp} \cdot \dot{m}_{hf}$, $\Delta T_{sh} \cdot T_{hf}$) were included to capture cross-variable coupling, while trigonometric or rational functions were excluded, as polynomial expansions are sufficient to describe the dominant nonlinearities within the observed operating envelope.

A total of $M = 231$ polynomial basis functions was generated from the regressor vector $\varphi(k)$ defined in (5). The resulting basis matrix is

$$\Phi(\varphi(k)) = \begin{bmatrix} \phi_1(\varphi(k)) & \phi_2(\varphi(k)) & \cdots & \phi_M(\varphi(k)) \end{bmatrix}, \quad (15)$$

where each $\phi_i(\varphi(k))$ corresponds to either a constant, linear, squared, or bilinear polynomial term derived from the lagged inputs and outputs. Representative examples include

$$c,\ \Delta T_{sh}(k-1),\ N_{pp}(k-2),\ T_{hf}(k-3),\ \dot{m}_{hf}(k-4),$$
$$\Delta T_{sh}(k-1)^2,\ N_{pp}(k-1)\cdot T_{hf}(k-2),\ \Delta T_{sh}(k-2)\cdot \dot{m}_{hf}(k-3),\ \ldots$$

A compact representation of $\Phi(\varphi(k))$ is shown in (16):

$$\Phi(\varphi(k)) = \begin{bmatrix} 1 \\ \varphi_1(k) \\ \varphi_2(k) \\ \varphi_1(k)^2 \\ \varphi_1(k)\varphi_2(k) \\ \vdots \end{bmatrix} \quad (16)$$

The identification dataset consisted of 4000 samples acquired at 1 Hz under closed-loop operation. To ensure persistence of excitation, the setpoints of the controlled variables were generated using broadband input signals. Specifically, the superheating setpoint was excited using an amplitude-modulated

pseudo-random binary sequence (AM–PRBS), the heat-source temperature setpoint combined a PRBS sequence with a low-amplitude multisine perturbation, and the heat-source mass-flow-rate setpoint followed a standard PRBS profile. These excitation patterns produced variations of $\Delta T_{\mathrm{sh}} \in [10, 32]$ K, $T_{hf} \in [108, 126]$ °C, and $\dot{m}_{hf} \in [1.45, 2.05]$ kg/s, covering the full operating envelope relevant for control. The closed-loop controller was tuned to maintain safe operation (e.g., preventing excessively low superheating values) while still allowing sufficiently rich excitation for identification. The complete 4000-sample sequence was used for model identification, and an entirely separate dataset was later used for validation. The input signals used for identification are depicted in Fig. 8.

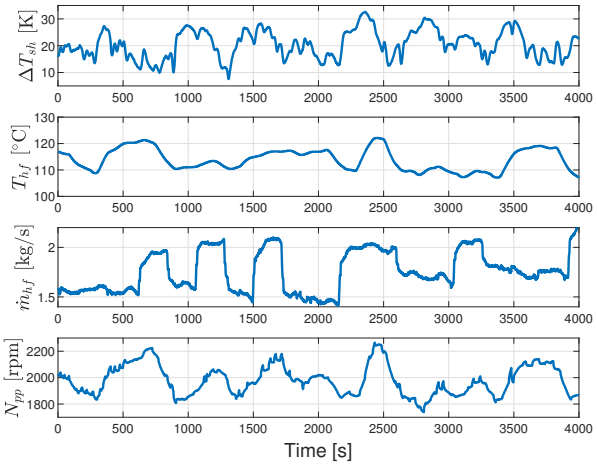

Figure 8: Input signals used for identification of the sparse nonlinear model.

The identification algorithm was implemented in MATLAB®, using the CVX toolbox [36] for convex optimization. The regressor orders were set to $n_a = n_b = 5$, and the sparsity tuning parameter ζ was swept from 1 to 3 to investigate the trade-off between the number of active basis functions and fitting performance on the identification dataset. The resulting trade-off curve is shown in Fig. 9.

A value of $\zeta = 1.4$ was selected as the best compromise, close to the knee of the sparsity–accuracy trade-off curve in Fig. 9, beyond which further reductions in model complexity lead to a disproportionate loss in fitting performance. This result highlights that accurate prediction of low superheating degree values requires a relatively large number of interaction terms. The corresponding coefficient magnitudes of the active basis functions are shown in Fig. 10, illustrating the sparse nature of the identified model.

For benchmarking purposes, three alternative modeling strategies from the literature were implemented: a linear model (LM), a piecewise linear (PWL) model, and a multiple-model Bayesian (MMB) approach. A brief description of each method is provided below.

4.2. Linear Model (LM)

The linear benchmark model is identified using the Prediction Error Method (PEM) [34] with multisine excitation. A

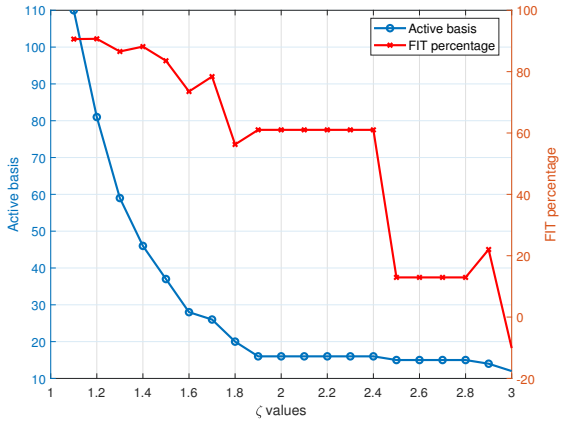

Figure 9: Impact of sparsity parameter ζ on the number of active basis functions (left axis) and FIT percentage (right axis), computed on the identification dataset.

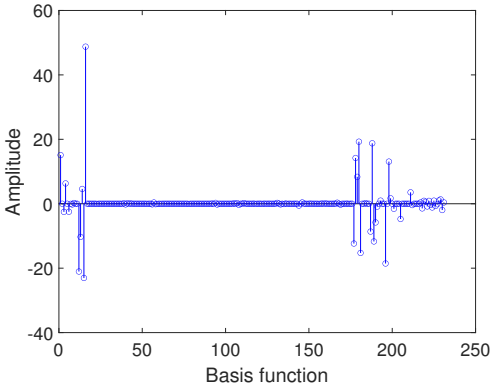

Figure 10: Coefficients of the active basis functions in the sparse nonlinear polynomial model.

sampling time of $T_s = 1$ s is selected to capture the system's fastest dynamics. In this formulation, the heat source temperature T_{hf} and mass flow rate $\dot{m}_{hf}$ are treated as *measured disturbances*—external inputs affecting ΔT_{sh} but not manipulated by the controller. The identified model thus describes the relationship between these disturbances, the control input N_{pp}, and the output ΔT_{sh}.

A separate open-loop dataset was used for identification to avoid bias introduced by feedback correlation in closed-loop operation. The nominal operating conditions for this experiment are listed in Table 1. This identification choice follows standard linear system identification practice and ensures that the linear model benchmark is obtained under conditions that are methodologically appropriate for PEM-based estimation.

The identified model is expressed as a discrete-time transfer function in compact MISO form:

$$\Delta T_{sh}(t) = \begin{bmatrix} G_{11}(q^{-1}) & G_{12}(q^{-1}) & G_{13}(q^{-1}) \end{bmatrix} \begin{bmatrix} N_{pp}(t) \\ T_{hf}(t) \\ m_{hf}(t) \end{bmatrix}. \quad (17)$$

This model is used here as a benchmark; full derivations of the transfer functions are reported in [8]. The normalized root-

Table 1: Nominal operating conditions during linear model identification

Parameter	*Description*	*Value*	*Unit*
N_{pp}	Pump speed	2100	rpm
N_{exp}	Expander speed	5000	rpm
$T_{sat,ev}$	Evaporating temperature	94	$^{\circ}C$
ΔT_{sh}	Superheating	15	K
T_{hf}	Heat source temperature	118	$^{\circ}C$
$\dot{m}_{hf}$	Heat source mass flow rate	1.7	kg/s
T_{cf}	Cold fluid temperature	24	$^{\circ}C$
$\dot{m}_{cf}$	Cold fluid mass flow rate	4	kg/s
$\dot{W}_{el,net}$	Net output power	6	kW
η_{cycle}	Cycle efficiency	6	%

mean-square error (NRMSE) on a validation dataset is approximately 70% (see (2)).

4.3. Piecewise Linear (PWL) Model

To extend the validity of linear models across a broader operating range, a piecewise linear (PWL) strategy is adopted. Several local linear models are identified under different heat source conditions, and their parameters are interpolated using surface maps. This methodology, described in detail in [8], is summarized here for completeness.

Based on step response analysis (Fig. 4), the dynamics of each local model are approximated using a First-Order Plus Time Delay (FOPTD) structure:

$$\frac{\Delta T_{sh}(s)}{N_{pp}(s)} = \frac{K_{\Delta T}}{\tau_{\Delta T} s + 1} e^{-T_d s}. \tag{18}$$

Parameter maps for the process gain $K_{\Delta T}$ and time constant $\tau_{\Delta T}$ are obtained as polynomial fits of ΔT_{sh} and $\dot{m}_{hf}$:

$$\begin{aligned} K_{\Delta T} = {} & p_{00} + p_{10}\Delta T_{sh} + p_{01}\dot{m}_{hf} + p_{20}\Delta T_{sh}^2 + \dots \\ & p_{11}\Delta T_{sh}\dot{m}_{hf} + p_{02}\dot{m}_{hf}^2 \end{aligned} \tag{19}$$

The time delay T_d is relatively small and treated as constant across the operating space. Discretization using the zero-order hold (ZOH) method yields a discrete-time representation suitable for prediction and control design. This PWL model serves as another benchmark for evaluating the proposed sparse nonlinear model.

4.4. Multiple Linear Model with Bayesian Selection (MMB)

To address the limitations of fixed-structure models like FOPTD—particularly under strong nonlinearities at low superheating degrees—a Multiple Model Bayesian (MMB) approach is considered [37]. This method combines a bank of N_m linear models with probabilistic weighting, allowing smooth transitions between local models as operating conditions vary.

The scheme, illustrated in Fig. 12, computes at each time step k the residuals

$$\varepsilon_i(k) = y(k) - \hat{y}_i(k),$$

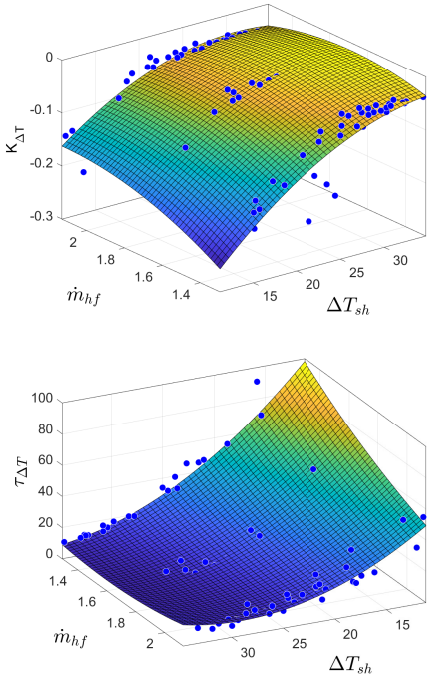

Figure 11: Gain and time constant maps as a function of superheating and heat source mass flow rate.

which are used to update model probabilities $P_{i,k}$ recursively via

$$P_{i,k} = \frac{\exp\left(-\frac{1}{2}\varepsilon_{i,k}^{\top}\mathbf{K}\varepsilon_{i,k}\right) P_{i,k-1}}{\sum_{j=1}^{N_m} \exp\left(-\frac{1}{2}\varepsilon_{j,k}^{\top}\mathbf{K}\varepsilon_{j,k}\right) P_{j,k-1}}, \tag{20}$$

where $\mathbf{K} = K\mathbf{I}$ adjusts the sensitivity of the weighting. A higher K smooths the blending between models, whereas a lower K accelerates convergence to a single dominant model.

Normalized weights are then computed as

$$w_{i,k} = \begin{cases} \dfrac{P_{i,k}}{\sum_{j=1}^{N_m} P_{j,k}}, & \text{if } P_{i,k} > \psi \\ 0, & \text{otherwise} \end{cases} \tag{21}$$

with $\psi = 1/N_m$ ensuring no model probability vanishes entirely.

The overall prediction is obtained as the weighted sum of all model outputs:

$$\hat{y}_{\text{avg}}(k) = \sum_{i=1}^{N_m} w_{i,k}\hat{y}_i(k). \tag{22}$$

The main implementation details of the multiple-model benchmark (MMB) are summarized here. The MMB relies on a bank of $N_m = 18$ local linear models, each identified from dedicated open-loop experiments conducted at distinct operating points spanning the relevant range of superheating, heat-source temperature, and heat-source mass flow rate. The local models are obtained using PRBS excitation and prediction-error identification, following the procedure experimentally validated in [37]. During operation, the contribution of each local model

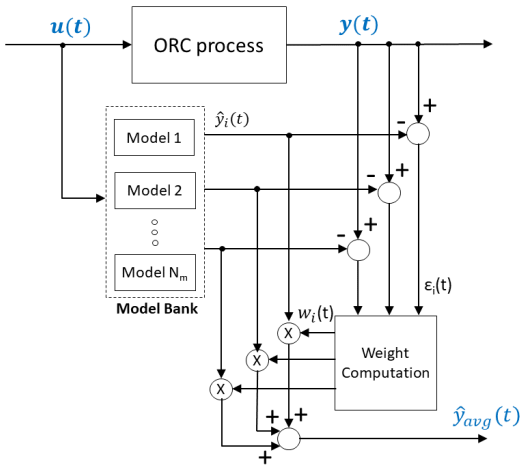

Figure 12: Schematic of multiple model structure with Bayesian selection.

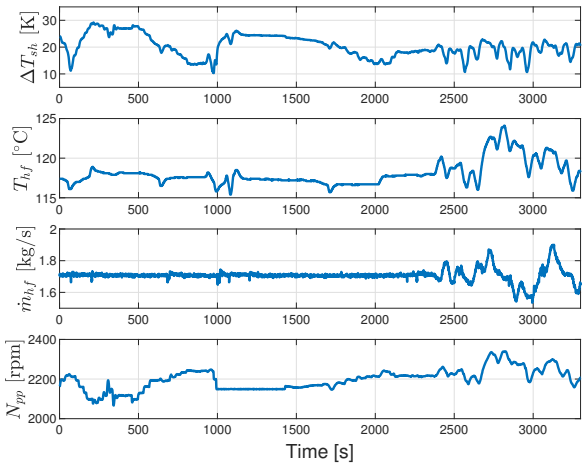

Figure 13: Inputs used for testing the prediction capabilities of the identified models.

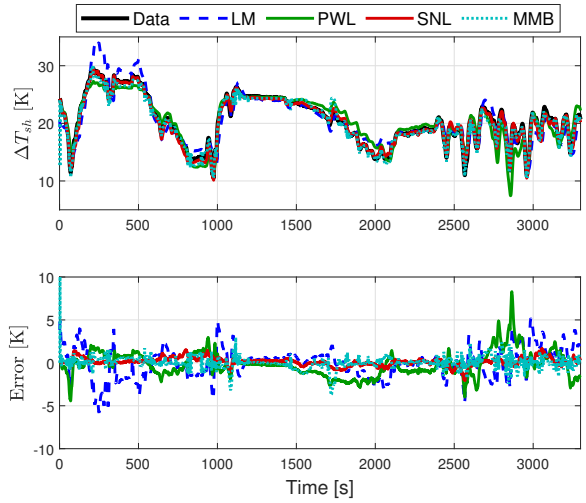

Figure 14: Prediction performance of LM (dashed blue), PWL (green), MMB (dotted cyan), and SNL (red) models for ΔT_{sh} on the validation dataset. Black: measured output.

is determined online using the recursive Bayesian weighting mechanism based on the prediction residuals. The resulting weights are normalized and used to compute the weighted average prediction, enabling smooth interpolation between models as operating conditions vary. The Bayesian tuning parameter governing the convergence and blending behavior of the model weights was selected as $K = 58$, which was shown to provide a suitable trade-off between fast convergence and robust blending in previous experimental studies [37].

This approach captures varying dynamics with low computational cost and provides another benchmark for performance comparison in the following section.

4.5. Performance comparison

The prediction capabilities of each model—Linear Model (LM), Piecewise Linear (PWL), Multiple Model Bayesian (MMB), and Sparse Nonlinear (SNL)—are evaluated on an independent dataset, distinct from that used for identification. This ensures an unbiased assessment of generalization performance under realistic operating conditions. The test sequence excites the system with variations in pump speed, heat source temperature, and mass flow rate, within the 10–30 K superheating range where nonlinear effects are most pronounced (see Section 2.2). The input signals for this validation are shown in Fig. 13.

The corresponding model predictions are compared with measured data in Fig. 14. As expected, the LM and PWL models exhibit the largest deviations, particularly when operating conditions move away from the nominal linearization point. The MMB and SNL approaches, which explicitly account for nonlinearities, track the measured dynamics more closely across the entire range.

Table 2 quantifies these results in terms of RMSE and FIT, using the definitions in (2)–(3). The LM benchmark achieves the lowest accuracy (FIT $\approx 58\%$), with the PWL model providing only a modest improvement (FIT $\approx 64\%$). In contrast, the MMB model attains 82.5% FIT, while the proposed SNL model achieves the highest accuracy at 88.1%. The latter corresponds to the optimal point on the ζ trade-off curve in Fig. 9 ($\zeta = 1.4$), confirming that the automatic tuning strategy from Section 3.4 effectively balances sparsity and prediction quality.

A more detailed view is obtained by analyzing three operating scenarios from Fig. 13. In **Scenario 1** (0–1000 s), the heat source is nearly constant and variations are driven primarily by pump speed changes. The LM model exhibits peak errors of about -5 K, underestimating the nonlinear gain at low superheating. The PWL model partially mitigates this but retains similar peak error. Both MMB and SNL significantly reduce the error, with SNL showing the smallest deviations.

In **Scenario 2** (1000–2000 s), all inputs remain nearly constant, producing slow dynamics. All models maintain errors within ± 3 K, despite being applied in free-run simulation mode without feedback correction.

Scenario 3 (2000–3000 s) is the most demanding, with simultaneous large changes in N_{pp}, T_{hf}, and $\dot{m}_{hf}$. Here, LM

Table 2: Comparison results for model predictions on the validation dataset (see Fig. 14). RMSE in Kelvin [K].

Identification method	RMSE [K]	FIT [%]
Linear Model (LM)	1.710	58.42
Piecewise Linear (PWL)	1.484	63.92
Multiple Model Bayesian (MMB)	0.719	82.52
Sparse Nonlinear Model (SNL)	0.488	88.13

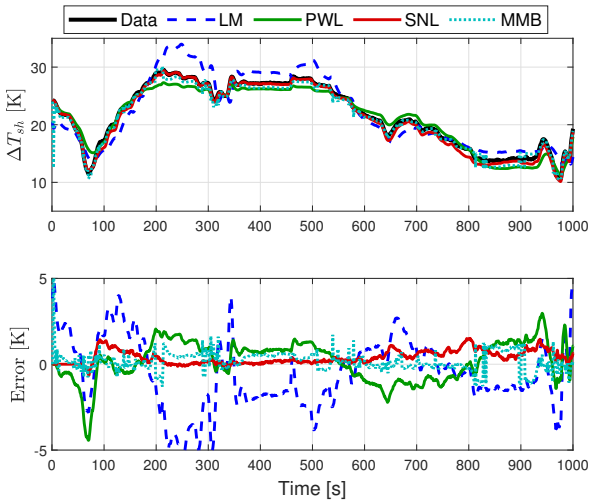

Figure 15: Performance comparison for Scenario 1.

and PWL fail to capture the coupled dynamics, with PWL performance further limited by its omission of T_{hf}. The MMB model adapts better, containing errors within $\pm 3\,\mathrm{K}$, but the SNL achieves the best tracking, with average error below $\pm 1.2\,\mathrm{K}$.

In addition to prediction accuracy, the computational cost associated with model evaluation is assessed to support real-time applicability. The average execution time in microseconds required to compute a one-step-ahead prediction is measured for each model over the validation dataset. The linear model (LM) required $4.45\,\mu$s per step, the piecewise linear model (PWL) $26.73\,\mu$s, the sparse nonlinear model (SNL) $204.52\,\mu$s, and the multiple-model Bayesian (MMB) approach $213.21\,\mu$s. These results indicate that the proposed SNL model achieves its improved accuracy with a computational cost comparable to MMB and well within the time scales typically required for real-time model predictive control in WHR-ORC applications.

Complementary to the online evaluation costs, the identification time is assessed to evaluate practical usability. On the considered dataset ($L = 4000$ samples, $M = 231$ candidate basis functions), the complete identification procedure, including sparsity parameter sweep ζ, convex optimization, and refinement, required approximately 320 s (i.e., on the order of 10^2 s) on a standard desktop computer (Windows 11, MATLAB 2023a, Intel(R) Core(TM) i5-9300H CPU @ 2.40 GHz, 16 GB RAM). As the identification is performed offline, this computational cost is acceptable for control-oriented modeling and does not impact real-time operation.

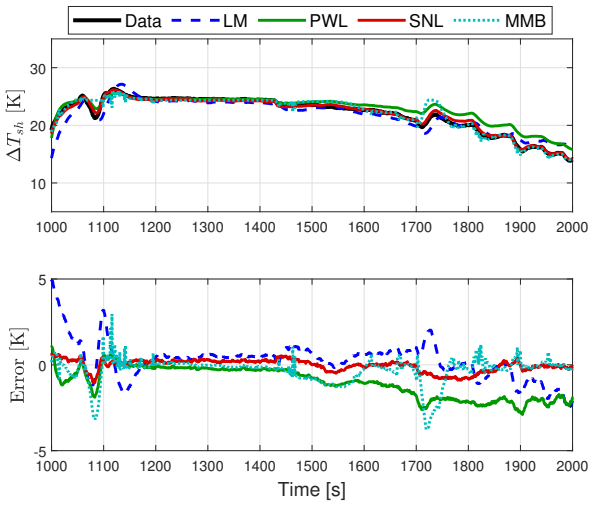

Figure 16: Performance comparison for Scenario 2.

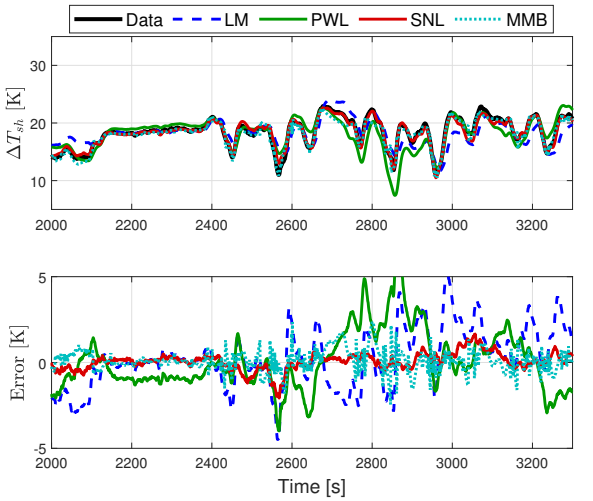

Figure 17: Performance comparison for Scenario 3.

Remark: These results confirm that the sparse nonlinear model not only achieves the best global accuracy, but also maintains robust performance under rapidly changing and highly coupled operating conditions—precisely the regimes where ORC systems are most sensitive to control errors. Its low complexity and physically interpretable structure (see Section 4.6) make it an attractive choice for model predictive control implementation.

4.6. Interpretation of Selected Basis Functions

An important advantage of the proposed sparse identification framework is that the resulting model structure is directly interpretable in physical terms. Table 3 classifies the $m_\theta = 46$ active basis functions obtained at the optimal sparsity setting ($\zeta = 1.4$) into four categories.

The dominant group consists of *bilinear* terms—products between different variables, often at different time lags—whereas the number of purely linear or squared terms is small, and no cubic or higher-order terms were retained. This reflects both

Table 3: Summary of selected basis function types in the sparse nonlinear model.

Term Type	Count	Example
Constant	1	c
Lagged linear	8	$N_{pp}(t-1)$
Squared	1	$\Delta T_{sh}(t-1)^2$
Multiplicative (bilinear)	36	$T_{hf}(t-4)\cdot\dot{m}_{hf}(t-2)$
Total	**46**	

the design of the candidate library (restricted to second-order polynomials for numerical robustness) and the natural effect of sparsity regularization, which tends to suppress redundant or weakly correlated terms.

From a thermodynamic perspective, the prevalence of bilinear terms is consistent with known ORC dynamics. The degree of superheating is strongly influenced by interactions between the working-fluid flow rate (linked to N_{pp}), the inlet heat-source temperature T_{hf}, and the heat-source mass-flow rate $\dot{m}_{hf}$. These interactions enter the governing heat-transfer equations multiplicatively, for example:

$$Q_{\text{in}} \propto \dot{m}_{hf}\, c_p \big(T_{hf} - T_{\text{ev,su}}\big).$$

In the discrete-time framework adopted for identification, such multiplicative relationships naturally manifest as products between lagged variables. Transport and thermal-inertia effects introduce delays between variations in T_{hf}, $\dot{m}_{hf}$, and ΔT_{sh}, so their influence on the measured output appears through time-shifted combinations such as $T_{hf}(t-j)\cdot\dot{m}_{hf}(t-i)$. Likewise, the coupling between pump-speed variations $N_{pp}(t-i)$ and the available heat-source temperature $T_{hf}(t-j)$ reflects the physical dependence of the evaporator heat input on both fluid flow and thermal power. The algorithm's preference for cross-variable products such as $N_{pp}(t-i)\cdot T_{hf}(t-j)$ or $\Delta T_{sh}(t-i)\cdot\dot{m}_{hf}(t-j)$ therefore mirrors the actual physics, where energy transfer results from the concurrent—but temporally shifted—interaction of flow and temperature fields.

The appearance of time-shifted products, for instance $T_{hf}(t-5)\cdot\dot{m}_{hf}(t-4)$, indicates that the model captures multi-time-scale effects typical of thermofluid systems. These effects originate from convective transport delays in the heat exchangers and from the thermal inertia of both the working fluid and the metallic structure, which cause heat-transfer interactions to manifest at different characteristic lags. Consequently, the identified structure reflects how changes in the heat-source conditions propagate dynamically through the ORC's thermal network.

The single squared term, $\Delta T_{sh}(t-1)^2$, suggests a mild nonlinear self-dependence in the superheating dynamics, but the absence of higher-order univariate terms reinforces the idea that cross-variable coupling dominates the system's nonlinear behavior. This observation aligns with the expected thermofluid behavior of ORC processes, in which coupled variations of flow and temperature govern energy transport more strongly than intrinsic nonlinearities in any single variable. Such coupling becomes particularly relevant at low superheating levels, where small perturbations in one variable (e.g., T_{hf} or $\dot{m}_{hf}$) can substantially amplify the response in another.

Overall, the final sparse polynomial model achieves a balance between *parsimony* and *physical interpretability*. By retaining only the most informative low-order interaction terms, the identification method avoids overfitting while preserving the essential structure of the ORC's heat-transfer and fluid-dynamic processes. This compact and physically meaningful representation makes the model well suited for real-time, model-based control applications where transparency and computational efficiency are essential.

5. Conclusions and Future Work

This paper presented a sparse nonlinear identification framework for modeling the superheating dynamics of a Waste Heat Recovery Organic Rankine Cycle (WHR-ORC) system. A globally valid nonlinear parametric model was identified from experimental data using a polynomial basis expansion with automatic structure selection and a guaranteed prediction error bound, formulated within a set-membership convex optimization framework.

Experimental validation on an 11 kW_{el} ORC test bench demonstrated that the proposed sparse nonlinear model achieves high prediction accuracy across a wide operating range while maintaining a compact structure. Compared to linear, piecewise linear, and multiple-model Bayesian benchmarks, the identified model exhibits superior generalization in strongly nonlinear and time-varying regimes, with a computational cost compatible with real-time control applications.

Beyond accuracy, the resulting model offers physical interpretability. The identified structure is dominated by bilinear interaction terms, revealing strong cross-couplings between operating variables that are consistent with the underlying thermodynamic behavior of ORC systems.

As with most sparse identification approaches, the proposed methodology has some limitations. The quality of the resulting model depends on the choice of the candidate basis function library, as unmodeled nonlinear interactions cannot be recovered. In addition, the set-membership formulation relies on the specification of noise bounds, which influences the sparsity–accuracy trade-off. Nevertheless, the automatic tuning strategy and sparsity-driven selection mitigate these effects by enabling the use of rich candidate libraries while retaining a compact final model. The framework is not inherently limited to single-input single-output systems and can, in principle, be extended to multiple-input multiple-output configurations, albeit at the cost of increased computational and modeling complexity.

Future work will focus on integrating the proposed model into nonlinear or robust model predictive control frameworks and extending the methodology to other thermodynamic and process systems exhibiting multivariable nonlinear dynamics.

References

[1] S. Quoilin, M. Van Den Broek, S. Declaye, P. Dewallef, V. Lemort, Techno-economic survey of organic rankine cycle (orc) systems,

Renewable and Sustainable Energy Reviews 22 (2013) 168–186. doi:10.1016/j.rser.2013.01.028.

[2] S. Lecompte, H. Huisseune, M. van den Broek, M. D. Paepe, Methodical thermodynamic analysis and regression models of organic rankine cycle architectures for waste heat recovery, Energy 87 (2015) 60 – 76. doi:http://dx.doi.org/10.1016/j.energy.2015.04.094.

[3] S. Gusev, D. Ziviani, I. Bell, M. De Paepe, M. Van den Broek, Experimental comparison of working fluids for organic rankine cycle with single-screw expander, in: In 15th International Refrigeration and Air Conditioning Conference at Purdue, Proceedings, 2014.

[4] H. Jouhara, N. Khordehgah, S. Almahmoud, B. Delpech, A. Chauhan, S. A. Tassou, Waste heat recovery technologies and applications, Thermal Science and Engineering Progress 6 (2018) 268 – 289. doi:https://doi.org/10.1016/j.tsep.2018.04.017.

[5] J. Sun, W. Li., Operation optimization of an organic rankine cycle (orc) heat recovery power plant, J. Applied Thermal Engineering Vol. 31 (2011) 2032–2041.

[6] B. Xu, D. Rathod, A. Yebi, Z. Filipi, A comparative analysis of real-time power optimization for organic rankine cycle waste heat recovery systems, Applied Thermal Engineering 164 (2020) 114442. doi:https://doi.org/10.1016/j.applthermaleng.2019.114442.

[7] J. Peralez, P. Tona, O. Lepreux, A. Sciarretta, L. Voise, P. Dufour, M. Nadri., Improving the control performance of an organic rankine cycle system for waste heat recovery from a heavy-duty diesel engine using a model-based approach, in: In IEEE Conference on Decision and Control, Florence, Italy, 2013.

[8] A. Hernandez, A. Desideri, S. Gusev, C. Ionescu, M. van den Broek, S. Quoilin, V. Lemort, R. De Keyser, Design and experimental validation of an adaptive control law to maximize the power generation of a small-scale waste heat recovery system, Applied Energy 203 (2017) 549–559.

[9] M. Imran, R. Pili, M. Usman, F. Haglind, Dynamic modeling and control strategies of organic rankine cycle systems: Methods and challenges, Applied Energy 276 (2020) 115537. doi:https://doi.org/10.1016/j.apenergy.2020.115537.

[10] S. Qin, T. Badgwell., A survey of industrial model predictive control technology., Control engineering practice 11 (2003) 733–764.

[11] J. Maciejowski., Predictive Control: With Constraints, Pearson Education, Prentice Hall, 2002.

[12] J. Berberich, J. Köhler, M. A. Müller, F. Allgöwer, Data-driven model predictive control with stability and robustness guarantees, IEEE Transactions on Automatic Control 66 (4) (2021) 1702–1717. doi:10.1109/TAC.2020.3000182.

[13] A. Dey, A. Dhar, S. Bhasin, Adaptive output feedback model predictive control, IEEE Control Systems Letters 7 (2023) 1129–1134. doi:10.1109/LCSYS.2022.3231837.

[14] S. Quoilin, R. Aumann, A. Grill, A. Schuster, V. Lemort., Dynamic modeling and optimal control strategy for waste heat recovery organic rankine cycles, Applied Energy Vol. 88 (2011) 2183–2190.

[15] A. Desideri, B. Dechesne, J. Wronski, M. Van Den Broek, S. Gusev, V. Lemort, S. Quoilin, Comparison of moving boundary and finite-volume heat exchanger models in the modelica language, submitted to energies (2016) 1–17.

[16] D. Rathod, B. Xu, Z. Filipi, M. Hoffman, An experimentally validated, energy focused, optimal control strategy for an organic rankine cycle waste heat recovery system, Applied Energy 256 (2019) 113991. doi:https://doi.org/10.1016/j.apenergy.2019.113991.

[17] W. R. Huster, A. M. Schweidtmann, A. Mitsos, Hybrid mechanistic data-driven modeling for the deterministic global optimization of a transcritical organic rankine cycle, in: S. Pierucci, F. Manenti, G. L. Bozzano, D. Manca (Eds.), 30th European Symposium on Computer Aided Process Engineering, Vol. 48 of Computer Aided Chemical Engineering, Elsevier, 2020, pp. 1765–1770. doi:https://doi.org/10.1016/B978-0-12-823377-1.50295-0.

[18] M. Lin, R. Chi, X. Yin, X. Liu, Model free adaptive control for organic rankine cycle processes, in: 2017 6th Data Driven Control and Learning Systems (DDCLS), 2017, pp. 542–546. doi:10.1109/DDCLS.2017.8068129.

[19] J. Zhang, X. Tian, Z. Zhu, M. Ren, Data-driven superheating control of organic rankine cycle processes, Complexity 2018 (1) (2018) 4154019. arXiv:https://onlinelibrary.wiley.com/doi/pdf/10.1155/2018/4154019, doi:https://doi.org/10.1155/2018/4154019.

[20] X. Wu, J. Qin, J. Chen, Y. Wang, Efficient predictive control method for orc waste heat recovery system based on recurrent neural network, Applied Thermal Engineering 257 (2024) 124352. doi:10.1016/j.applthermaleng.2024.124352.

[21] M. S. Turgut, Neural koopman operator-assisted model predictive control of an Organic Rankine Cycle, Applied Thermal Engineering (2023). doi:10.1016/j.applthermaleng.2023.12345678.

[22] Y. Shi, Z. Zhang, X. Chen, L. Xie, X. Liu, H. Su, Data-driven model identification and efficient mpc via quasi-linear parameter varying representation for orc waste heat recovery system, Energy 271 (2023) 126959. doi:10.1016/j.energy.2023.126959.

[23] Q. Zhang, L. Wang, W. Xu, H. Su, L. Xie, Nonlinear sparse variational bayesian learning based model predictive control with application to pemfc temperature control, Control Engineering Practice 148 (2024) 105952. doi:https://doi.org/10.1016/j.conengprac.2024.105952.

[24] S. A. Billings, Nonlinear System Identification: NARMAX Methods in the Time, Frequency, and Spatio-Temporal Domains., Wiley, 2013.

[25] C. Novara, Sparse identification of nonlinear functions and parametric set membership optimal analysis., in: in proc. American control conference, San Francisco, USA, 2011.

[26] R. Tibshirani, Regression shrinkage and selection via the lasso, Journal of the Royal Statistical Society, Series B 58 (1994) 267–288.

[27] H. Zou, T. Hastie, Regularization and variable selection via the elastic net, Journal of the Royal Statistical Society, Series B 67 (2005) 301–320.

[28] A. R. Ugolini, V. Breschi, A. Manzoni, M. Tanelli, Sindy vs hard nonlinearities and hidden dynamics: a benchmarking study, IFAC-PapersOnLine 58 (15) (2024) 49–54, 20th IFAC Symposium on System Identification SYSID 2024. doi:https://doi.org/10.1016/j.ifacol.2024.08.503.

[29] A. Hernandez, F. Ruiz, A. Desideri, C. Ionescu, S. Quoilin, V. Lemort, R. De Keyser, Nonlinear identification and control of organic rankine cycle systems using sparse polynomial models, in: 2016 IEEE Conference on Control Applications (CCA), 2016, pp. 1012–1017. doi:10.1109/CCA.2016.7587946.

[30] M. Tanaskovic, L. Fagiano, C. Novara, M. Morari, Data-driven control

of nonlinear systems: An on-line direct approach, Automatica 75 (2017) 1–10. doi:https://doi.org/10.1016/j.automatica.2016.09.032.

[31] F. Valderrama, F. Ruiz, Limited-complexity controller tuning: A set membership data-driven approach, European Journal of Control 58 (2021) 82–89. doi:https://doi.org/10.1016/j.ejcon.2020.07.002.

[32] V. Lemort, A. Zoughaib, S. Quoilin., Comparison of control strategies for waste heat recovery organic rankine cycle systems, In Sustainable Thermal Energy Management in the Process Industries International Conference (SusTEM2011) (2011).

[33] A. Hernandez, A. Desideri, C. Ionescu, S. Quoilin, V. Lemort, R. De Keyser., Experimental study of predictive control strategies for optimal operation of organic rankine cycle systems., in: Proceedings of the European Control Conference (ECC15), Linz, Austria, 2015.

[34] L. Ljung, System identification: theory for the user, Prentice-Hall, 2007.

[35] C. Novara, Sparse identification of nonlinear functions and parametric set membership optimality analysis, IEEE Transactions on Automatic Control 57 (12) (2012) 3236–3241. doi:10.1109/TAC.2012.2202051.

[36] M. Grant, S. Boyd, CVX: Matlab software for disciplined convex programming, version 2.1, `http://cvxr.com/cvx` (Mar. 2014).

[37] A. Hernandez, F. Ruiz, S. Gusev, R. De Keyser, S. Quoilin, V. Lemort, Experimental validation of a multiple model predictive control for waste heat recovery organic rankine cycle systems, (Submitted for publication in Applied Thermal Engineering) (2020).